Polymer Testing 28 (2009) 196–203

Contents lists available at ScienceDirect

Polymer Testing

journal homepage: www.elsevier.com/locate/polytest

Test Method

On the nonlinear evolution of the Poisson's ratio under quasi-static loading for a carbon fabric-reinforced thermoplastic. Part I: Influence of the transverse strain sensor

I. De Baere*, W. Van Paepegem, J. Degrieck

Department of Materials Science and Engineering, Faculty of Engineering, Ghent University, Sint-Pietersnieuwstraat 41, B-9000 Gent, Belgium

ARTICLE INFO

Article history:
Received 27 October 2008
Accepted 11 December 2008

Keywords:
Composite
Carbon fibre
Polyphenylene sulphide
Poisson's ratio

ABSTRACT

When observing or describing the damage state in a composite material, often only Young's modulus or residual deformation are considered. Generally, however, the Poisson's ratio is more sensitive to damage than those properties. Rather than observing the Poisson's ratio as a function of crack density, this article studies the evolution of the Poisson's ratio as function of the longitudinal strain, which has a peculiar shape. In Part I, multiple experiments, using strain gauges, optical fibres and an extensometer for transverse strain measurement are discussed to determine whether this behaviour is due to the material or to the sensor used. It can be concluded that the hyperbolic-like shape is entirely caused by material behaviour. A theoretical explanation and validation for this behaviour will be given in part II.
The material used for this study is a carbon fabric-reinforced PPS.

1. Introduction

There are a number of articles in the literature which mention the fact that, generally, the Poisson's ratio is more sensitive to damage than Young's modulus or residual (or permanent) deformation [1–5]. The decrease in the Poisson's ratio is usually explained by the occurrence of transverse cracks, causing elongation in the longitudinal direction. These transverse cracks originate from failure in the transverse plies, but the cracks remain open, causing the elongation, because of the release of thermal (or residual) stresses resulting from the curing or production process [6–10].

For the carbon fabric-reinforced polyphenylene sulphide considered in this paper, these thermal or residual stresses will be relatively high because of (i) the negative thermal expansion coefficient in the fibre direction of the carbon-reinforcement, (ii) the semi-crystalline nature of the PPS and (iii) the processing temperatures for thermoplastics are higher compared to the curing temperatures for thermosets. Hence, due to the existence of large thermal stresses in the material under study, the Poisson's ratio is expected to show a decreasing trend and will, therefore, be an interesting parameter for damage monitoring.

When modelling the evolution of the Poisson's ratio, it is always plotted as a function of (transverse) crack density [1–4]. Of course, for fibre-reinforced epoxies, this approach may work just fine; the evolution of cracks can be easily visualised, even without the need for penetrant enhanced radiography. However, if the Poisson's ratio is used to monitor and model damage during (fatigue) experiments, it would seem more convenient to model this behaviour as function of the occurring stress or strain state. Also, determining the crack density is quite cumbersome. Therefore, in this article, it is assessed whether the Poisson's ratio can be used to monitor any

* Corresponding author. Tel.: +32 (0)9 264 32 55; fax: +32 (0)9 264 35 87.
E-mail address: ives.debaere@ugent.be (I. De Baere).

0142-9418/$ – see front matter © 2008 Elsevier Ltd. All rights reserved.
doi:10.1016/j.polymertesting.2008.12.002

damage degradation under quasi-static cyclic loading conditions, and its behaviour as a function of the strain state will be studied. To the best of the authors' knowledge, such results have not yet been published in open literature. The second part of this study [16] will give an analytical explanation of the peculiar ν_{12}–ε_{xx} behaviour, which is found here.

In Section 2, the material and equipment are described. This is followed by a short overview of the experiments, after which a discussion is given. Finally, some conclusions are drawn.

2. Materials and methods

2.1. Composite material

The material under study was a carbon fibre-reinforced polyphenylene sulphide (PPS), called CETEX. This material was supplied to us by Ten Cate. The fibre type is the carbon fibre T300J 3K and the weave pattern is a 5-harness satin weave with a mass per surface unit of 286 g/m^2. The 5-harness satin weave is a fabric with high strength in both directions and excellent bending properties.

The carbon PPS plates were hot pressed, only one stacking sequence was used for this study, namely $[(0^\circ, 90^\circ)]_{4s}$ where $(0^\circ, 90^\circ)$ represents one layer of fabric.

The in-plane elastic properties of the individual carbon PPS lamina were determined by the dynamic modulus identification method as described in [11] and are listed in Table 1.

The tensile strength properties were determined at the Technical University of Delft and are listed in Table 2.

The test coupons were sawn with a water-cooled diamond saw. The dimensions of the coupons are shown in Fig. 1 and the geometry of the end tabs was chosen according to the result from [12].

2.2. Equipment

All tensile tests were performed on a servo-hydraulic INSTRON 8801 tensile testing machine with a FastTrack 8800 digital controller and a load cell of ±100 kN. The quasi-static tests were displacement-controlled with a speed of 2 mm/min. For the alignment of the grips, AlignPro™ from INSTRON was used.

For the registration of the tensile data, a combination of a National Instruments DAQpad 6052E for fireWire, IEEE 1394 and the SCB-68 pin shielded connector were used. The load, displacement and strain, given by the FastTrack controller, as well as the extra signals from strain gauges were sampled on the same time basis.

Table 1
In-plane elastic properties of the individual carbon/PPS lamina (dynamic modulus identification method).

E_{11}	56.0	GPa
E_{22}	57.0	GPa
ν_{12}	0.333	–
G_{12}	4.175	GPa

Table 2
Tensile strength properties of the individual carbon/PPS lamina (Mechanical testing at TUDelft).

X_T	734.0	MPa
ε_{11}^{ult}	0.011	–
Y_T	754.0	MPa
ε_{22}^{ult}	0.013	–
S_T	110.0	MPa

3. Experiments and discussion

3.1. Introduction

For this study, a large number of quasi-static hysteresis tests were performed, of which some are illustrated in this paper and some will be given in Part II [16]. Such a quasi-static hysteresis tests consist of a number of successive tensile tests: the specimen is loaded until a certain stress level is reached, after which the specimen is unloaded. This is repeated a number of times, during which the maximum stress level is increased or kept constant. The general idea is that during the loading certain damage processes take place, and it is assumed that during the unloading no extra damage growth occurs. The effects of the damage mechanics are then visualised by unloading the specimen and determining certain parameters, such as Young's modulus, permanent deformation or, in this case, the Poisson's ratio.

Since all experiments performed showed similar results, only a few are illustrated in this paper. For a more detailed overview of the experiments, readers are referred to [13].

3.2. Quasi-static test

Before starting with the quasi-static cyclic tests, it is first verified whether this material indeed shows a decreasing Poisson's ratio. Two experiments are shown here, the specimens were loaded at 2 mm/min until failure and both the longitudinal and transverse strains were measured using strain gauges. Their positions are indicated in Fig. 1.

In Fig. 2, the evolution of the stress σ_{11} as a function of the strain ε_{11} is given. It may be concluded that this material has a linear behaviour up to failure. The failure stresses are 643.5 MPa for G4 and 594.3 MPa for G7. These low values compared to Table 2 are due to premature failure in the tabs. Young's modulus can also be derived from these

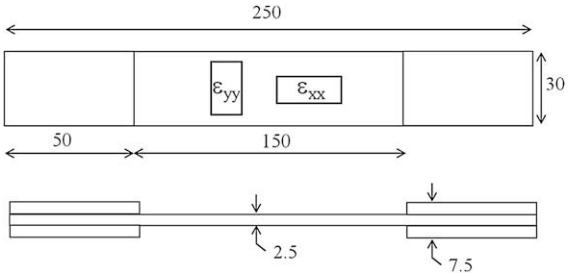

Fig. 1. Dimensions of the used tensile coupon, equipped with straight-end tabs of $[(0^\circ, 90^\circ)]_{4s}$ carbon/PPS [12].

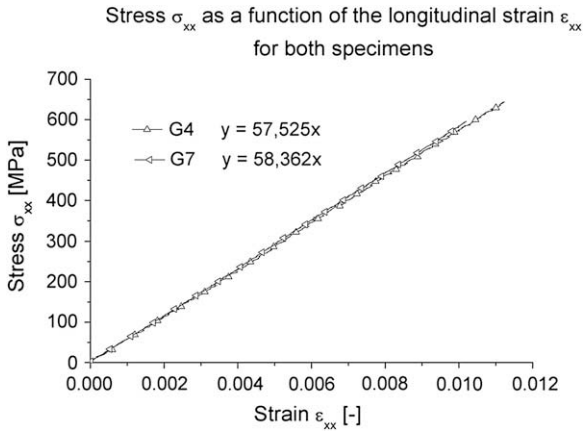

Fig. 2. σ_{11} as a function of ε_{xx} for both specimens.

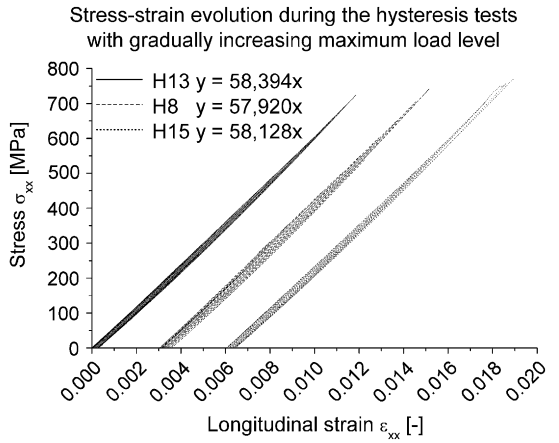

Fig. 4. Stress as function of the strain for the quasi-static hysteresis test with increasing load level.

experiments, a value of 57.5 GPa for G4 and 58.4 GPa for G7 are found. These values show good agreement with the values in Table 1.

Fig. 3 shows the evolution of Poisson's ratio as a function of the longitudinal strain. An average value of 0.049 and 0.053 is found for G4 respectively G7. This value also shows good correspondence with the values found with the resonalyser technique (Table 1).

It may be noted that once the longitudinal strain exceeds about 0.006, the ratio tends to decrease. At fracture, ν_{12} is only about 60% of its original value, namely 0.035 for G4 and 0.03 for G7. This decrease in the Poisson's ratio may present the possibility of using ν_{12} as a means of characterizing damage. This, however, is examined by the quasi-static cyclic tests, which are discussed next.

3.3. Strain gauge measurements

For the first series of tests, standard strain gauges were mounted to measure the longitudinal and transverse strain, as illustrated in Fig. 1. Fig. 4 shows the stress–strain evolution for three specimens H8, H13 and H15. For a clear representation, the different curves are given a longitudinal strain offset of 0.003. For each test, the first loading level was 100 MPa and for every next cycle, the load was increased by 50 MPa. This was continued until failure.

For specimen H13, 14 cycles were done and the specimen failed during the fourteenth cycle at 730 MPa. Specimen H8 endured 15 cycles and failed during the last cycle at 741 MPa. Specimen H15 lasted 13 cycles, the cycle of 650 MPa was omitted, and it failed at 760 MPa. It can be noticed that there is no stiffness degradation and only very limited permanent deformation. As such, these two parameters are not very suitable for monitoring the damage state in the material. It should be noted that the derived stiffness again corresponds well with the values given in Table 1.

The longitudinal and transverse strain for the test on specimen H15 are shown in Fig. 5; similar results were found for all other experiments.

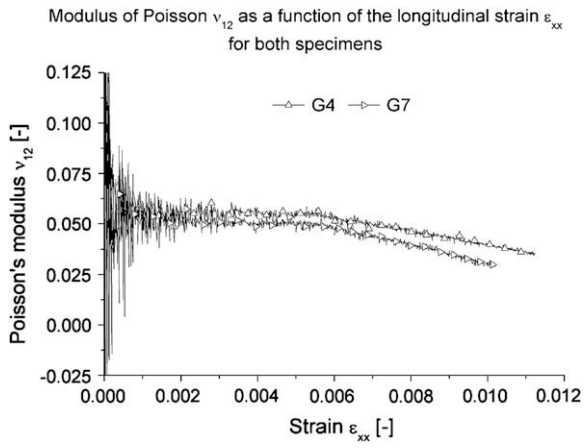

Fig. 3. ν_{12} as a function of ε_{11} for both specimens.

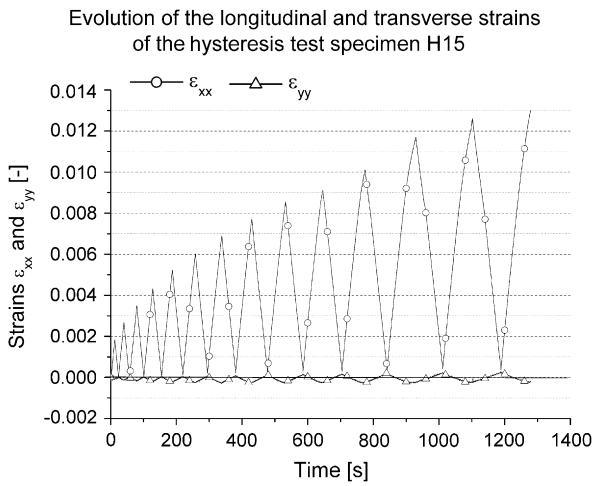

Fig. 5. Evolution of ε_{xx} and ε_{yy} as a function of time for the hysteresis test on H15.

It should be noted that the transverse strain ε_{yy} becomes positive after unloading, which would result in a negative value of the Poisson's ratio. This can be verified in Fig. 6, where the evolution of Poisson's ratio is depicted for the same specimen.

It can be noticed that there is a decreasing trend in the Poisson's ratio at maximum load, as indicated by the 'loading' arrow. An initial value of about 0.05 is found, which corresponds well with the previously derived values, and at failure the Poisson's ratio has decreased to 0.02. Therefore, this is a promising parameter for monitoring damage.

However, as can be seen in Fig. 6, the evolution of Poisson's ratio as a function of the longitudinal strain has a peculiar hyperbolic-like shape; it must be mentioned that the loading curve of cycle $i+1$ is always below the unloading curve of cycle i.

In order to assess whether this behaviour is caused by some form of electrical hysteresis of the strain data-acquisition system, a few tests were conducted where, prior to the hysteresis loadings, starting from 100 MPa with increasing maximum load level, four cycles to 100 MPa were performed. This value should be low enough not to induce any damage in the material, so if the effect is the result of the data acquisition, it should be visible. Again, various experiments were performed, all with similar results, so only one is depicted. The evolution of the Poisson's ratio as function of the longitudinal strain for such an experiment (specimen H13) is shown in Fig. 7. Of course, there is some scatter in the Poisson's ratio for very small strains but, once the signal is stabilized, the 'diving' effect does not occur and for the four cycles the value of the Poisson's ratio does remain constant at a value of about 0.05, which corresponds with the previously derived values. This constant value also confirms that the maximum stress level of 100 MPa is low enough not to induce damage.

A possible cause of the 'diving' effect may be the testing speed. All previous tests were done with a displacement speed of 2 mm/min. To rule out any possible visco-elastic effects of the matrix, the next experiment was done at

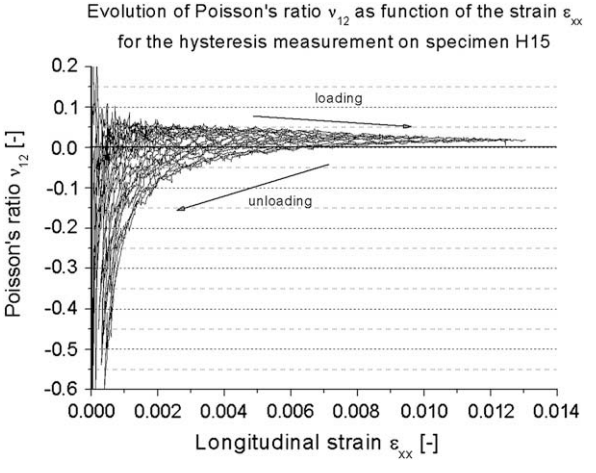

Fig. 6. The evolution of Poisson's ratio as function of the longitudinal strain.

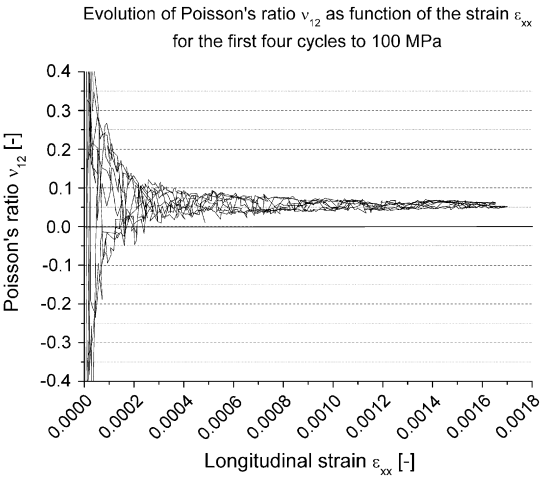

Fig. 7. The evolution of Poisson's ratio as function of the longitudinal strain for the first four cycles to 100 MPa.

0.1 mm/min. Furthermore, two transverse strain gauges were used, one on each side of the specimen, to rule out the effects of torsion or buckling due to misalignment of the clamps. The latter, however, is unlikely because the grips were aligned using the INSTRON AlignPro system. Because of the low testing speed, only three cycles up to 100 MPa were done, after which the maximum load of each cycle was increased by 100 MPa. This resulted in five cycles and a maximum stress of 600 MPa, because then the tabs started to de-bond.

The evolution of the strains for the first three cycles is shown in Fig. 8. There is a very good correspondence between both transverse strain gauges, meaning no buckling or torsion due to misalignment of the clamps is present. Furthermore, the transverse strain does not become positive.

The corresponding evolution of the Poisson's ratio, for both transverse strain gauges, shows the same evolution as in Fig. 7 and, therefore, is not illustrated here. Apart from

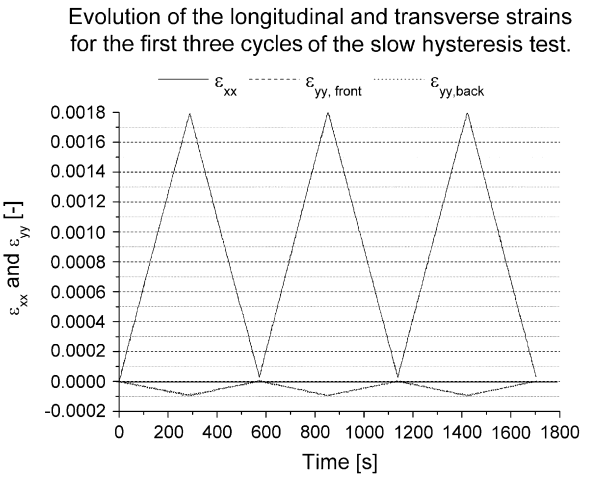

Fig. 8. Evolution of ε_{xx} and ε_{yy} as a function of time for the first cycles of the slow hysteresis test.

the scatter due to the very low strain levels, no diving is present; an initial value of 0.05 is found in accordance with the previously determined values.

The evolution of the strains for the cycles with increasing maximum load is depicted in Fig. 9. Again, there is a very good correspondence between the two transverse strain gauges, except for the last cycle. This may be explained by the de-bonding of the tabs causing bending of the specimen due to the asymmetrical load introduction. This also causes the nonlinear behaviour of the longitudinal strain ε_{xx} for the last cycle.

Despite the slow displacement speed, the transverse strain still becomes positive for both strain gauges, which would mean that the typical diving also occurs for this testing speed. This can be verified from Fig. 10, which shows the evolution of the Poisson's ratio for both the transverse strain gauges. It should be noted that both curves correspond well, except for the last cycle, because of the de-bonding of the tabs.

3.4. Transverse external optical fibre

In the previous section, it was investigated whether the typical shape of the ν_{12}–ε_{xx} curve was due to the displacement speed or to a possible misalignment of the grips, but this was not the case. However, this shape may also result from the strain gauge sensor. Therefore, a similar experiment was performed but with a transverse optical fibre bonded to the surface of the specimen. For comparison purposes, a transverse train gauge was also used for the transverse strain measurement.

The optical fibre was externally bonded using Z70 adhesive and the optical data-acquisition system was the FBG-scan interrogator. This means that the experiment was done under load control with stepwise loadings. More specific details on how to use external optical fibres, e.g. how the fibre is bonded to the surface and details on the data acquisition can be found in [14].

First, three loading cycles up to 100 MPa were performed and then the maximum stress was gradually increased by 50 MPa for each cycle.

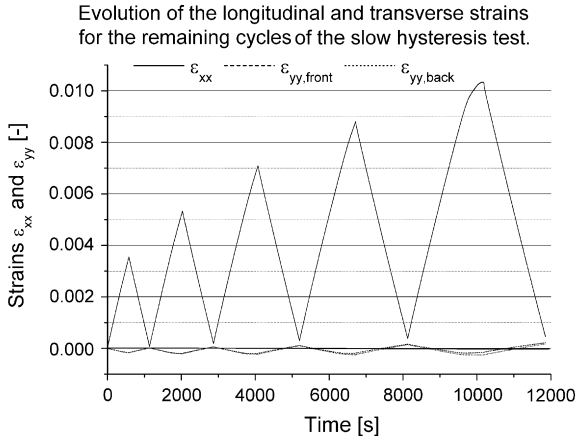

Fig. 9. Evolution of ε_{xx} and ε_{yy} as a function of time for the remaining cycles of the slow hysteresis test.

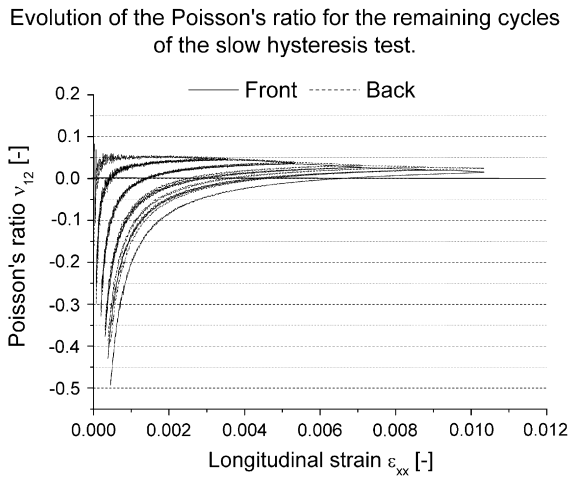

Fig. 10. The evolution of Poisson's ratio as function of the longitudinal strain for the remaining cycles.

Fig. 11 illustrates the evolution of the transverse strain measured with both the strain gauge and the optical fibre sensor. It can be seen that the correspondence is very good.

The corresponding evolution of the Poisson's ratio as function of the longitudinal strain is similar to the one depicted in Fig. 7 and, therefore, it is not shown here. An initial value of 0.06 was found, which is in good agreement with the previously derived values.

While performing the cyclic loading with increasing maximum stress level, it was noted that for the higher strain levels the optical fibre measurement started to show 'sparks'. This is illustrated in Fig. 12, which shows the transverse strains for the cycles from 150 MPa up to 250 MPa. It should be noted that despite these 'sparks' the correspondence still is very good.

The 'sparking' effect is due to the occurrence of multiple peaks in the reflected spectrum, which is caused by inhomogenous straining of the grating [15]. If the bond between

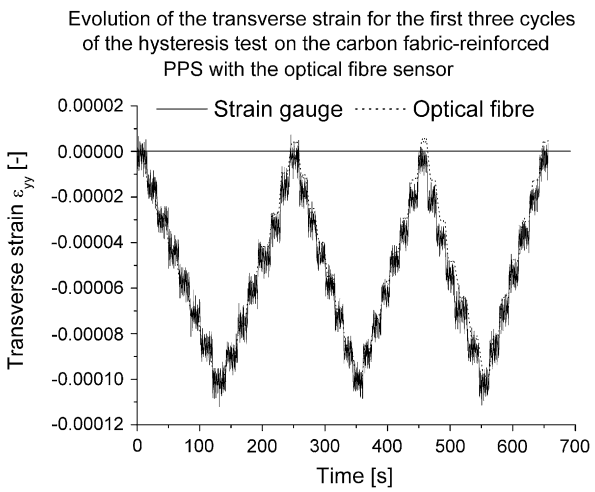

Fig. 11. Evolution of ε_{yy} for both the optical fibre as strain gauge measurement, as a function of time for the first three cycles.

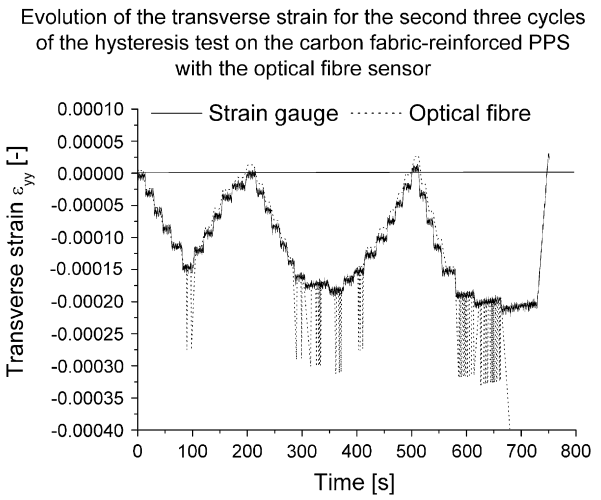

Fig. 12. Evolution of ε_{yy} for both the optical fibre as strain gauge measurement, as a function of time for the second three cycles.

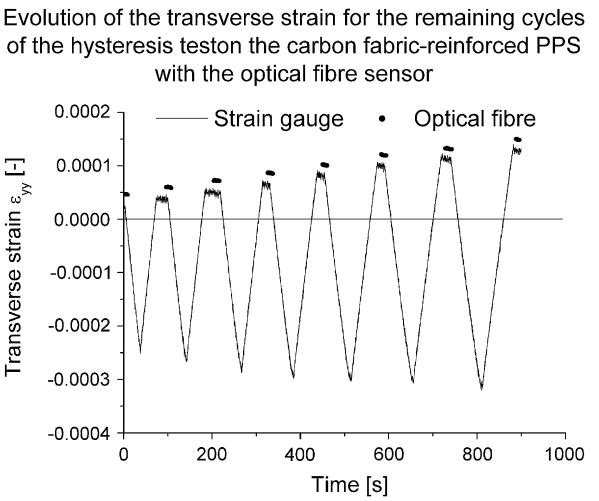

Fig. 14. Evolution of ε_{yy} for both the optical fibre as strain gauge measurement, as a function of time for the remaining cycles.

the fibre and the specimen's surface is not perfect, as is the case here, then this will result in a varying strain field, causing 'peak-splitting'. This was experimentally verified for this specimen and is shown in Fig. 13. The specimen was loaded until a certain stress level and a screenshot of the entire spectrum was taken. For the lower stress levels, only one peak was seen, but for higher stress levels, multiple peaks occurred.

The peak used for the strain measurement in Fig. 12 is the one to the right in Fig. 13. Since it is shifted to the right, this explains the sudden 'increase' in strain in Fig. 12.

More details on the peak-splitting of the optical fibre for the material under study can be found in [13].

Since the purpose of this test was mainly to verify if the transverse strain becomes positive after cyclic loadings, causing the negative Poisson's ratio, and since the 'peak-splitting' does not occur for low stress levels, the experiment was continued and the optical fibre was only read when the stress was equal to zero. The resulting evolution of the transverse strains for the remaining cycles from 300 MPa to 600 MPa is depicted in Fig. 14. Considering the fact that the measured strains are very low, there is a good agreement between the strain gauge and the optical fibre in the unloaded condition.

Finally, Fig. 15 shows the evolution of the Poisson's ratio as function of the longitudinal strain for the strain gauge measurement. As could be expected, again the peculiar behaviour is visible, as well as the decreasing value of ν_{12} at maximum load level.

3.5. Transverse extensometer

The two previously used sensors have one thing in common. They are both bonded to the surface using an adhesive. Of course, the origin of this peculiar evolution of the Poisson's ratio may be due to the adhesive. Therefore,

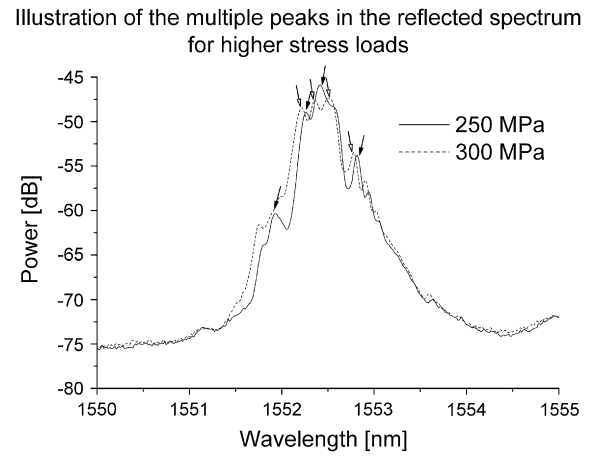

Fig. 13. Reflected spectra of the externally bonded optical fibre for higher stress levels.

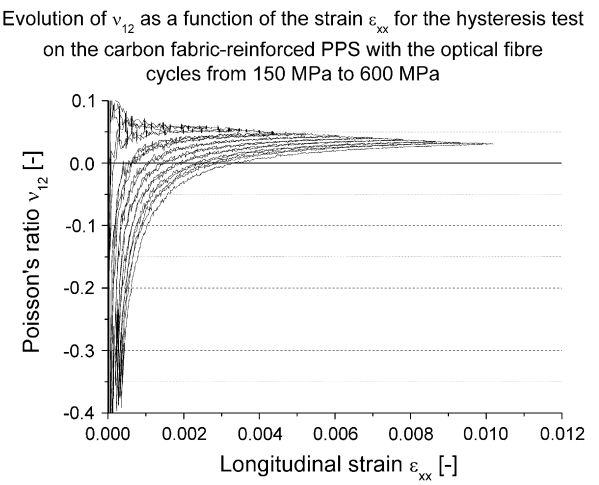

Fig. 15. The evolution of Poisson's ratio as function of the longitudinal strain for the strain gauge measurements for the loading cycles between 150 MPa and 600 MPa.

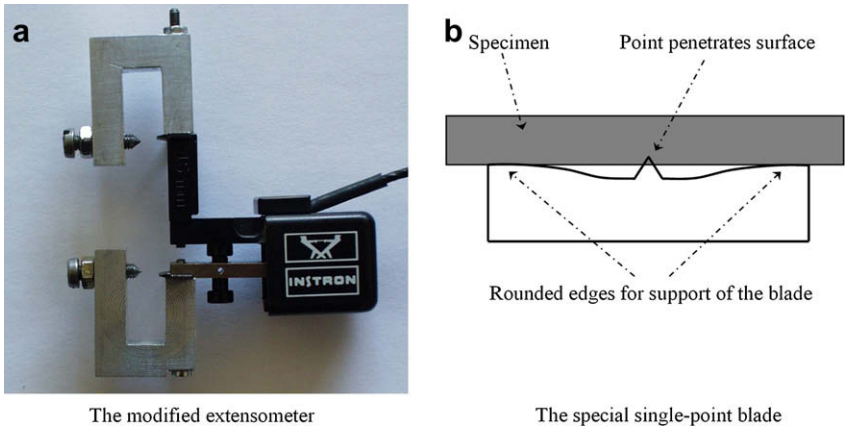

Fig. 16. The standard INSTRON extensometer, modified to measure transverse strain.

the standard longitudinal extensometer was adjusted, so that it can measure the transverse strain. This of course requires some adjustments for the extensometer, which are discussed next.

Two U-shaped pieces are used to mount the extensometer around the specimen. Two pointed bolts are used to press the extensometer blades against the specimen. Since preliminary tests showed that the standard blades, which make a line contact, tend to slide, two new blades were made which each make contact with the surface on one discrete point, exactly opposite to the pointed bolts. Of course, if the extensometer tilts a little bit, the single-point contact cannot prevent this, so the outer edges of the blade are rounded for support, but they cannot penetrate the surface. As such, the strain is measured between two discrete points and the longitudinal strain has no influence on the measurement. The modifications can be seen in Fig. 16.

A few experiments were done, again with similar results, so only one is illustrated here. This test was done starting at 100 MPa and for each cycle, the maximum stress was increased by 50 MPa; the displacement speed was 2 mm/min. The test was stopped after 550 MPa was reached, since failure of the specimen could damage the extensometer.

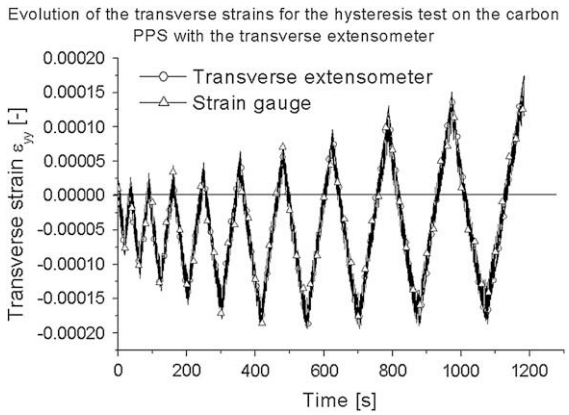

Fig. 17. Evolution of ε_{yy} for both the extensometer as strain gauge measurement, as a function of time.

Fig. 17 shows the evolution of the transverse strain, measured with both the transverse extensometer and the strain gauge. It can be seen clearly that both signals correspond perfectly. This has two very important consequences. First, this means that the peculiar behaviour of the Poisson's ratio as a function of the longitudinal strain is due to the material, rather than the used sensor. Second, this proves that the transverse extensometer is capable of measuring the (very) small transverse strains accurately. As such, the transverse extensometer could also be used to measure the transverse strains in fatigue experiments, which is a very important advantage, since the extensometer will not de-bond after a certain number of cycles, which often occurs for transverse strain gauges.

Again, a similar evolution of the Poisson's ratio as depicted in Figs. 6, 10 and 15 is found.

4. Conclusions

From all experiments discussed above, it can be concluded that the carbon fabric-reinforced polyphenylene sulphide shows no stiffness degradation and only limited permanent deformation occurs. When cyclic loadings with increasing maximum stress are applied, the permanent deformation also increases with each load.

With respect to the Poisson's ratio, a decreasing value is found. Similar to the permanent deformation, ν_{12} continuously decreases with increasing maximum load cycles and the different cycles can clearly be distinguished.

Furthermore, the evolution of the Poisson's ratio as a function of the longitudinal strain has been studied. A very peculiar shape of this curve was found and it was assessed whether the hyperbolic-like shape was due to the sensor, used to measure the transverse strain. As such, measurements were done using transverse strain gauges, transverse optical fibres with Bragg gratings and a transversely mounted extensometer. It could be concluded that the typical behaviour is caused by the material itself rather than by the used sensor. It was also confirmed that the testing speed did not have any influence on this behaviour and that alignment was perfect.

Acknowledgements

The authors are highly indebted to the university research fund BOF (Bijzonder Onderzoeksfonds UGent) for sponsoring this research and to Ten Cate Advanced Composites for supplying the material. They would also like to thank Luc Van den Broecke, for his assistance in the laboratory and Chris Bonne, for his help with the strain gauge measurements.

References

[1] F. Gao, L. Boniface, S.L. Ogin, P.A. Smith, R.P. Greaves, Damage accumulation in woven-fabric CFRP laminates under tensile loading: Part 1. Observations of damage accumulation, Composites Science and Technology 59 (1) (1999) 123–136.
[2] M. Surgeon, E. Vanswijgenhoven, M. Wevers, O. Van der Biest, Transverse cracking and Poisson's ratio reduction in cross-ply carbon fibre-reinforced polymers, Journal of Materials Science 34 (22) (1999) 5513–5517.
[3] F. Gao, L. Boniface, S.L. Ogin, P.A. Smith, R.P. Greaves, Damage accumulation in woven-fabric CFRP laminates under tensile loading: 2. Modelling the effect of damage on macro-mechanical properties, Composites Science and Technology 59 (1) (1999) 137–145.
[4] P.A. Smith, J.R. Wood, Poisson ratio as a damage parameter in the static tensile loading of simple crossply laminates, Composites Science and Technology 38 (1) (1990) 85–93.
[5] P.P. Parlevliet, H.E.N. Bersee, A. Beukers, Residual stresses in thermoplastic composites – a study of the literature. Part III: Effects of thermal residual stresses, Composites Part A: Applied Science and Manufacturing 38 (6) (2007) 1581–1596.
[6] L. DiLandro, M. Pegoraro, Evaluation of residual stresses and adhesion in polymer composites, Composites Part A: Applied Science and Manufacturing 27 (9) (1996) 847–853.
[7] F. Bassa, L. Boniface, K. Jones, S.L. Ogin, On the behaviour of the residual strain produced by matrix cracking in cross-ply laminates, Composites Part A 29 (A) (1998) 1425–1432.
[8] P.P. Parlevliet, H.E.N. Bersee, A. Beukers, Residual stresses in thermoplastic composites—a study of the literature—Part I: formation of residual stresses, Composites Part A: Applied Science and Manufacturing 37 (11) (2006) 1847–1857.
[9] M. Senel, H. Akbulut, M. Toparli, Residual stress analysis in symmetric thermoplastic laminated plates under thermal loads: analytic solution, Journal of Thermoplastic Composite Materials 17 (6) (2004) 481–507.
[10] C. Filiou, C. Galiotis, In situ monitoring of the fibre strain distribution in carbon-fibre thermoplastic composites 1. Application of a tensile stress field, Composites Science and Technology 59 (14) (1999) 2149–2161.
[11] I. De Baere, W. Van Paepegem, J. Degrieck, H. Sol, D. Van Hemelrijck, A. Petreli, Comparison of different identification techniques for measurement of quasi-zero Poisson's ratio of fabric reinforced laminates, Composites A 38 (9) (2007) 2047–2054.
[12] I. De Baere, W. Van Paepegem, J. Degrieck, On the design of end tabs for quasi-static and fatigue testing of fibre-reinforced composites, Polymer Composites. in press. doi:10.1002/pc.20564.
[13] I. De Baere, Experimental and numerical study of different setups for conducting and monitoring fatigue experiments of fibre-reinforced thermoplastics, Ph.D. thesis, Ghent University, Gent, Belgium, 2008. ISBN: 978-90-8578-196-7.
[14] I. De Baere, G. Luyckx, E. Voet, W. Van Paepegem, J. Degrieck, On the feasibility of optical fibre sensors for strain monitoring in thermoplastic composites under fatigue loading conditions, Optics and Lasers in Engineering. in press. doi:10.1016/j.optlaseng.2008.01.001.
[15] L. Sorensen, T. Gmur, J. Botsis, Residual strain development in an AS4/PPS thermoplastic composite measured using fibre Bragg grating sensors, Composites Part A: Applied Science and Manufacturing 37 (2) (2006) 270–281.
[16] I. De Baere, W. Van Paepegem, J. Degrieck, On the nonlinear evolution of the Poisson's ratio under quasi-static loading for a carbon fabric-reinforced thermoplastic. Part II: analytical explanation. Polymer Testing, submitted for publication.